A role of villin-dependent F-actin organization in peroxisome motility in Arabidopsis cells

Calvin H. Huang [a], Amanda M. Koenig [b], Yuh-Ru Julie Lee [a], Yibo Shi [a], Jianping Hu [b,c,1], Bo Liu [a,1]

[a] Department of Plant Biology, College of Biological Sciences, University of California, Davis, CA 95616, U.S.A.

[b] Michigan State University-Department of Energy Plant Research Laboratory, Michigan State University, East Lansing, MI 48824, U.S.A.

[c] Department of Plant Biology, Michigan State University, East Lansing, MI 48824, U.S.A.

[1] Corresponding authors: Bo Liu, bliu@ucdavis.edu; Jianping Hu, huji@msu.edu

Short title: Villins and peroxisome motility

ABSTRACT

Actin microfilaments (F-actin) serve as the track for directional movement of organelles in plants. To understand how the F-actin network is employed for the movement of peroxisomes, essential organelles in plant metabolism, we analyzed mutants of three villin (*VLN*) genes, which encode the primary actin-bundling factor and are most actively expressed in vegetative tissues in *Arabidopsis thaliana*. We found that the *vln4* mutation greatly exacerbated the growth and subcellular defects in *vln2 vln3*. Compared to the wild-type cells, the double and triple *vln* mutants exhibit progressive reduction of stable F-actin bundles and rapid remodeling of the fine filaments. The defective F-actin network did not prevent peroxisomes from taking on both rapid and slow movements along the tracks but caused significantly reduced speed of movement and displacement distance of peroxisomes. Using a correlation analysis method, we classified the complex heterogeneous peroxisome movement patterns into clusters reflecting distinct movement directionalities. The *vln* triple mutant had significantly reduced number of peroxisomes with long-range and linear movement. Our results provide insights into how VLN-dependent F-actin organization is coupled with the complex pattern of peroxisome movement.

INTRODUCTION

The single-membrane organelle peroxisome displays rapid directional movement through the cytoplasm while performing essential functions such as detoxification, β-oxidation, and phytohormone biosynthesis. All these functions likely require peroxisome translocation throughout the cell to scavenge cytotoxins and coordinate with other cellular compartments for versatile metabolic reactions (Sandalio et al., 2021). In mammals, peroxisomes interact with the endoplasmic reticulum (ER), lipid droplets, lysozymes, and mitochondria during metabolic processes like fatty acid catabolism, and defects in peroxisomal distribution and inter-organellar interactions are the underlying cause of several diseases in humans (Wanders et al., 2023). In plants, peroxisomes also exhibit critical interactions with chloroplasts for photorespiration and phytohormone biosynthesis, besides their interaction with the ER and mitochondria (Koenig et al., 2023; Pan et al., 2020). Additionally, peroxisomes participate in functions across the entire expanse of the cell, and their trafficking and spatial arrangement are often linked to the fluctuating demands of the cell during development or under stresses (He et al., 2021). The dynamic distribution of peroxisomes, therefore, requires agile motility along the cytoskeletal filaments and their associated motor proteins (Neuhaus et al., 2016).

In fungi and animals, peroxisome trafficking is primarily governed by microtubules and the associated motors of dynein and kinesins (Covill-Cooke et al., 2021; Salogiannis and Reck-Peterson, 2017). In plants, however, active movement of peroxisomes and other organelles predominately takes place on the F-actin tracks and depends on the motor proteins in the Myosin XI subfamily (Avisar et al., 2008). In *Arabidopsis thaliana*, for example, actin depolymerization or inactivation of multiple Myosin XI genes causes a nearly complete cessation of organelle movement (Mathur et al., 2002; Peremyslov et al., 2010). However, research to date has barely explored the molecular mechanisms that regulate actomyosin-dependent organelle movement in plants (Koenig et al., 2023). In typical differentiated plant cells, F-actin is organized into two distinct populations: long and stable bundles and highly dynamic filaments (Henty-Ridilla et al., 2013). It is unclear whether organelles like peroxisomes employ either or both types of F-actin tracks for their directional movement.

F-actin bundling in plants is primarily mediated by the villin (VLN) family proteins, which were initially isolated from lily pollen as abundant actin-binding proteins (Huang et al., 2015; Yokota et al., 2003). In Arabidopsis, VLN proteins are encoded by five genes and show various degrees of actin bundling capabilities both *in vitro* and *in vivo* (Li et al., 2025). Of the five paralogs, *VLN2*,

VLN3 and *VLN4* are most broadly expressed in vegetative tissues. The *vln2 vln3* double mutants display a reduction in F-actin bundling and altered growth patterns with twisted organs, but no significant compromise in vegetative growth (Bao et al., 2012; van der Honing et al., 2012). Therefore, we hypothesized that VLN4 might function redundantly with VLN2 and VLN3 in mediating organelle movement and the coupled growth processes in plants. Here, we analyzed F-actin organization and peroxisome movement in the mutants of these three Arabidopsis *VLN* genes highly expressed in vegetative tissues. The *vln2 vln3 vln4* triple mutant showed greatly reduced F-actin bundling, increased mesh-like F-actin networks, and gross defects in vegetative growth, which allowed us to interrogate how compromised F-actin bundling impacts patterns of peroxisome movement without disassembling the entire F-actin network. Our analysis of the *vln* triple mutant uncovered significantly reduced movement speed and decreased displacement distance of peroxisomes. We also developed quantitative methods to differentiate features associated with peroxisomal movement modes and correlate such differences with the varied F-actin organization patterns.

RESULTS

F-actin organization is deficient in the *vln* mutants

Although peroxisomes are known to move along F-actin tracks by Myosin XI motors in plant cells, it is unknown how the arrangement of the F-actin network facilitates modes of motility, specifically directional movement. We sought to understand the role of actin organization, particularly F-actin bundling, in peroxisome movement. Since the VLN proteins contribute significantly to actin bundling in plants (Huang et al., 2015), we used Arabidopsis *vln* mutants to address how F-actin bundling might be linked to peroxisome movement. Of the five Arabidopsis *VLN* paralogs, *VLN2*, *VLN3* and *VLN4* are most broadly expressed in vegetative tissues according to community-generated transcriptional data (https://bar.utoronto.ca/eplant/). It has recently been reported that VLN2, VLN3, and VLN4 function redundantly in hypocotyl elongation, with VLN2 playing the most prominent role, and that higher-order *vln* mutants display aberrant actin organization in the root and leaf cells (Li et al., 2025). Therefore, we predicted that these three VLN proteins function redundantly to regulate organelle movement and the coupled growth processes.

101 To determine the role of VLN in peroxisome dynamics, we isolated a *vln4* T-DNA homozygous
102 mutant from the ABRC (Arabidopsis Biological Research Center) and crossed it with the *vln2*
103 *vln3* (*vln2/3*) double mutant (Bao et al., 2012). This independently generated *vln2 vln3 vln4*
104 (*vln2/3/4*) triple mutant displayed growth defects (Supplemental Figure 1) similar to what was
105 described recently (Li et al., 2025).

106 Because of the reported impact of actomyosin-dependent cell growth and the defect of
107 hypocotyl cell elongation in the *vln2/3/4* mutant (Li et al., 2025), we used hypocotyl cells to
108 characterize the actin defects in more detail before investigating peroxisomal dynamics in the
109 mutants. Using live-cell imaging of F-actin labeled by a LifeAct-GFP (green fluorescent protein)
110 fusion protein, we first confirmed that F-actin cable formation is compromised in hypocotyl cells
111 in both the double and triple *vln* mutants (Figure 1A). Compared to the wild-type (WT) cells in
112 which thick, continuous F-actin bundles spanned the cell length, fine F-actin filaments in the *vln*
113 mutant cells were more prominent and organized into mesh-like networks (Figure 1A). In
114 addition, F-actin bundles are less frequently observed in *vln2/3* and completely absent in the
115 *vln2/3/4* triple mutant (Figure 1A). We further quantified the reduction of actin bundles in *vln*
116 hypocotyl cells using the parameter skewness, a standard metric used for assessing F-actin
117 bundling, in which higher fluorescence intensity of the LifeAct-GFP signal in bundled filaments
118 resulted in a higher skewness value (Higaki, 2017; Higaki et al., 2010). The *vln2/3* and *vln2/3/4*
119 mutants exhibited progressively reduced skewness compared to the WT, indicating decreased
120 F-actin bundling in the mutant cells (Figure 1B).

121 In WT cells, prominent F-actin cables are often oriented in parallel to the cell elongation axis,
122 likely underlying the recently reported cell elongation phenotype in *vln* mutant hypocotyls (Li et
123 al., 2025). To further assess the deficient F-actin network in the hypocotyl of the *vln* mutants, we
124 quantified the average angle of F-actin filaments, with 0° being in the transverse direction (as a
125 reference axis) and 90° being parallel to the growth direction (Figure 1A). In epidermal cells of
126 the WT hypocotyl, due to the presence of longitudinal bundles along the growth direction, the F-
127 actin filaments were more parallel to the direction of growth, as indicated by a higher average
128 angle (Figure 1C). In the *vln2/3* and *vln2/3/4* mutant cells, however, the overall angles became
129 smaller, concomitant with the decrease in long F-actin cables and the increasingly abundant
130 appearance of mesh networks of F-actin (Figure 1C).

131

132 **The dynamic and cell-spanning organization of F-actin is maintained in *vln* mutants**

133 Although *vln* mutants are deficient in actin bundling, they retain a reorganized F-actin network,
134 unlike complete elimination of the filaments by pharmacological means. Therefore, we
135 hypothesized that some actin-dependent organelle motility might be maintained in the mutants.
136 To better understand the specific actin structure available for cargo transport, we further
137 characterized the F-actin network in the *vln* mutants—using stability, coherency, and density as
138 the metrics.

139 Generally, thick F-actin fibers tend to be stable over time, whereas actin filaments in the mesh
140 network are more dynamic (Henty-Ridilla et al., 2013). Because the F-actin mesh network is
141 pronounced in the *vln2/3* and *vln2/3/4* mutants, we tested whether the altered array organization
142 was associated with rapid actin remodeling in these mutants. Images of F-actin were captured
143 at 5-sec intervals, after which images of different timepoints were pseudo-colored and merged.
144 Noticeably, while F-actin in WT cells predominantly appeared as 'white' in the merged images,
145 indicating little, if any, remodeling, the mutant cells showed more dynamic changes in F-actin
146 organization with each timepoint observed in discrete colors (Figure 2A). Further, the white color
147 in the merged images often correlated with thick, long F-actin bundles that are more static than
148 those filaments in the mesh networks in the same WT cells (Figure 2A). In the *vln2/3* and
149 *vln2/3/4* mutant cells, the three distinct colors were more evidently discerned (Figure 2A).
150 Likewise, quantification of F-actin stability showed that a significantly higher proportion of F-
151 actin in the *vln* mutants underwent remodeling than in the WT, with the *vln2/3/4* mutant cells
152 containing significantly fewer F-actin cables than *vln2/3* (Figure 2B). Our data supported
153 previous conclusions that loss of these three VLN proteins severely impaired F-actin bundling
154 and additionally demonstrated the predominance of a diffuse, dynamic mesh network of F-actin
155 in the high-order *vln* mutants.

156 Coherency is a measure of the degree of isotropy of the F-actin distribution, where 0 indicates
157 entirely random orientation and 1 indicates uniform orientation, the latter of which is
158 characteristic of cells enriched with actin cables. F-actin filaments in WT cells are organized in a
159 pattern with higher coherence values compared to the presence of more disordered filaments
160 with coherence closer to 0 in the *vln2/3* and *vln2/3/4* mutants (Figure 2C). The decreased
161 coherency in the *vln* mutants suggests the increased occurrence of dispersed and mesh F-actin
162 resulted from the reduced presence of cell-spanning F-actin bundles.

163 To further characterize the more diffuse, less linear F-actin network in *vln* mutants, we quantified
164 the density of F-actin by measuring the percentage of F-actin occupancy in the cytoplasm. The
165 *vln2/3* cells exhibited significantly higher F-actin occupancy than the WT cells, and the F-actin

166 density in *vln2/3/4* was approximately double that of the WT (Figure 2D). The increased F-actin
167 occupancy suggests that the F-actin network, despite being devoid of obvious bundles, still
168 spans the cortex in the mutants. Therefore, the cytoskeletal apparatus capable of supporting
169 organelle motility across the whole cell seems to persist in the mutants.

170 To determine if the VLN proteins are associated with F-actin, we expressed a VLN2-GFP fusion
171 protein under the control of its own promoter in the *vln2/3* double mutant. Suppression of the
172 mutant growth phenotype (Supplemental Figure 2A) suggests that VLN2-GFP is functional.
173 When co-expressed with LifeAct-mScarlet-I in tobacco cells, VLN2-GFP was mostly detected on
174 F-actin bundles (Supplemental Figure 2B). Similarly, A VLN4-GFP fusion protein expressed
175 under its native promoter also decorated F-actin bundles marked by LifeAct-mScarlet-I when
176 transiently expressed in tobacco cells (Supplemental Figure 2B).

177 Taken together, our data showed that in the *vln* mutants, F-actin dynamic polymerization and
178 cell-spanning organization are maintained while only cable formation is deficient. As such, these
179 knockout mutants can serve as an informative genetic tool to study the role of actin organization
180 in peroxisome motility.

181

182 **VLN-dependent actin bundling facilitates peroxisome movement**

183 Because of their intact F-actin filaments yet compromised F-actin bundles, the *vln* mutants
184 seemed to be an ideal system to evaluate the specific contribution of actin bundling to
185 peroxisome motility. To determine the impact of actin bundling in peroxisome movement and
186 distribution in Arabidopsis, we transformed WT, *vln2/3*, and *vln2/3/4* plants with constructs for
187 the markers of F-actin (LifeAct-GFP) and peroxisomes (mScarlet-I-SRL). Peroxisomes and F-
188 actin were visualized simultaneously in the hypocotyl cells of plants co-expressing the two
189 fusion proteins. The transgenic *vln* double and triple mutants exhibited progressive deficiencies
190 in F-actin bundling, resembling what was observed earlier in this study (Figure 3A). These
191 defects were concomitant with the progressive aggregation of peroxisomes, suggesting an
192 inability of peroxisomes to be distributed uniformly across the cell in the mutants (Figure 3A).
193 Maximum projections using the time dimensions are shown. It is worth noting that peroxisomes
194 of WT and occasionally in *vln2/3* mutants were able to make long, linear tracks across the cell
195 whereas peroxisomes in *vln2/3/4* moved mostly within a confined area (Figure 3A). Time-lapse
196 images, taken at 5-sec intervals in epidermal cells of the hypocotyl, revealed that peroxisomes
197 maintained motility along the F-actin tracks in both *vln2/3* and *vln2/3/4* mutants (Figure 3A,

198 Movie S1). Moreover, each track of peroxisome movement was heterogenous, with some rapid
199 movements (>1.5 μm/s) as well as more frequently observed slower movements (<0.5 μm/s),
200 similar to what was observed in the WT (Figure 3B), indicating that the mechanisms of
201 actomyosin-dependent peroxisome movement were at least partially maintained in the *vln*
202 mutants.

203 To examine the role of VLNs in peroxisome motility in more depth, we compared the speed of
204 peroxisome movement among WT, *vln2/3* and *vln2/3/4*. Despite variations in instantaneous
205 speed during imaging duration, calculation of the mean speed of each peroxisome movement
206 revealed that only the severe inhibition of F-actin bundling in *vln2/3/*4 caused a significant
207 decrease in the mean speed, while intermediate bundling in *vln2/3* was sufficient to maintain
208 peroxisome speed comparable to that of the WT (Figure 3B). These data suggest that
209 peroxisome movement is facilitated by both discrete F-actin filaments and densely bundled actin
210 cables.

211 Next, we wanted to exclude peroxisomes that were potentially unable to associate with F-actin
212 via myosin from our calculation and only assess the movement of peroxisomes already
213 associated with myosin motors. To achieve this goal, we calculated the maximum speed of
214 peroxisome movement, defined as the highest instantaneous speed recorded between two
215 consecutive timepoints. Again, the maximum speed distributions were not significantly different
216 between WT and *vln2/3*, but were more frequently observed at lower values in *vln2/3/4* (Figure
217 3C). We therefore conclude that actin dynamics and organization influence peroxisome velocity
218 and distribution.

219

220 **Fast, directional peroxisome movement and distribution are facilitated by F-actin cables**

221 Since the heterogenous pattern of peroxisome motility shifted towards slower speeds in the
222 absence of longitudinal actin bundles, as shown in the *vln2/3/4* triple mutants, we hypothesized
223 that F-actin cables specifically facilitate fast, linear movement, enabling uniform peroxisome
224 distribution across the cell. To test this, we evaluated total moving distance, displacement,
225 straight-line speed, overall linearity of movement, and directional change rate of peroxisomes
226 when they deviated from the prior trajectories (Figure 4A-E).

227 Measurement of the total moving distance revealed that most peroxisomes traverse similar
228 distances with no significant difference between mutant and WT cells (Figure 4A). However,

229 peroxisomes in *vln2/3/4* cells have a significantly shorter displacement, measured as the
230 shortest distance between the start and end points of a tracked peroxisome (Figure 4B).
231 Consistently, the triple mutant also exhibited reduced displacement distance, whose value was
232 normalized by track duration and represented by “straight-line speed” that accounts for any
233 variations of movements tracked per peroxisome (Figure 4C). Together these data suggest that,
234 while peroxisomes still move in short bursts that sum to a similar distance observed between *vln*
235 mutants and WT, these organelles do not successively travel as far distance in the *vln2/3/4*
236 mutant, which lacks prominent F-actin bundles or cables, when compared to WT or *vln2/3*. In
237 fact, peroxisomes in *vln2/3/4* mutant cells changed direction more frequently than those in the
238 WT cells. Motility in *vln2/3/4* was overall less linear with a lower ratio of straight-line speed to
239 track mean speed (Figure 4D). However, peroxisomes in the triple mutant more frequently
240 change directions (Figure 4E), likely because their movement predominantly relied on the
241 dynamic F-actin mesh network rather than stable, longitudinal bundles as tracks.

242 To better assess the heterogenous motility pattern of peroxisomes, we employed a Pearson’s
243 correlation matrix to conduct pairwise analysis of the influence of the aforementioned motility
244 parameters on each other within individual genotypes. The *vln* mutants showed correlations
245 comparable to WT between average velocity, maximum speed, total distance and track
246 displacement. By contrast, correlations between parameters that account for directional
247 movement (straightforward speed, linearity, and directional change rate) varied across
248 genotypes (Supplemental Figure S3A). We then plotted the data of straight-line speed, linearity,
249 and directional change rate from all genotypes in a 3-dimensional scatterplot and used k-means
250 clustering to group organelle motility according to these multidimensional criteria (Figure 5A).
251 Using the Elbow Plot method (Supplemental Figure S3B), the data were grouped into 3 clusters:
252 high straightforward speed and linearity but low directional change rate as Cluster 1;
253 intermediate straightforward speed, linearity, and directional change as Cluster 2; and low
254 straightforward speed and linearity but high directional change rate as Cluster 3. Cluster 1 is
255 enriched for peroxisomes that rapidly and directionally traverse the cell with minimal turns, while
256 Cluster 3 represented peroxisomes that move in short bursts with frequent changes in direction.
257 Interestingly, WT peroxisomes exhibited uniformly heterogeneous movement across the three
258 clusters, with roughly one third of the tracked movements represented in each cluster (Figure
259 5A). However, in the *vln2/3* mutants, a smaller proportion (29.6% in Cluster 1) of peroxisomes
260 move directionally compared to 32.8% in the WT, and the peroxisome motility profiles shifted
261 towards intermediate (Cluster 2) and short burst (Cluster 3) movements (Figure 5A). In the
262 *vln2/3/4* triple mutant, the reduction in fast, linear peroxisome movements was further

263 exacerbated (20.6% in Cluster 1), with more peroxisomes moving in short bursts (39.8%,
264 Cluster 3) compared to 30.5% in WT (Figure 5A). This shift in cluster populations across
265 genotypes suggests that a lesser proportion of peroxisomes move quickly and linearly when F-
266 actin bundling is deficient in the *vln* mutants.

267 To assess whether peroxisome distribution was altered in *vln* mutants, we determined the ratio
268 of track displacement to directional change rate. A higher ratio indicates greater dispersion, as it
269 reflects directed movement for a greater distance (*i.e.*, more displacement with few directional
270 changes). In contrast, a lower ratio reflects movement within a more confined region,
271 representing frequent directional changes with little displacement. In WT and to some extent
272 *vln2/3* mutants, long and stable F-actin cables serve as the track for peroxisomes to be
273 dispersed throughout the cell. However, the absence of such cables in *vln2/3/4* would limit
274 peroxisomes to move predominantly within localized regions. In agreement with this prediction,
275 the outcome of our quantification assessments indicated that the WT and *vln2/3* cells exhibited
276 higher average dispersion ratios [40.76 ± 5.10 and 50.8 ± 5.92 μm/(rad/sec), respectively] than
277 those of *vln2/3/4* [22.48 ± 0.97 μm/(rad/sec)] (Figure 5B). These findings suggest that
278 peroxisome movement becomes more confined within the actin mesh network in the triple
279 mutant.

280 Taken together, our results showed that densely bundled F-actin cables are necessary for rapid,
281 directional movement of peroxisomes, which likely enable the proper subcellular distribution of
282 peroxisomes required for their diverse metabolic functions.

283

284 **DISCUSSION**

285

286 In this work, we generated *vln2/3/4* triple mutant to investigate the collective roles of three F-
287 actin bundling VLN proteins in the dynamics and organization of the F-actin network. Our
288 quantitative analysis of peroxisome motility in the WT and *vln* mutants showed that VLN-
289 dependent F-actin organization is required for rapid directional movement of peroxisomes in the
290 epidermal cells of Arabidopsis hypocotyls.

291 Plant VLN proteins are grouped into three classes, in which VLN4 belongs to class III while
292 VLN2 and VLN3 are in class II (Khurana et al., 2010). Consistent with what was reported
293 recently (Li et al., 2025), we found loss of VLN4 to greatly enhance defects in the *vln2/3* double

294 mutant. Our results collectively indicate that the functions of these three VLN proteins, despite
295 being in two different classes, converge towards stabilizing F-actin and promoting high-order F-
296 actin bundle formation in vegetative tissues. However, when the three VLN proteins were
297 examined individually without an F-actin marker, they exhibited different extents of localization
298 on F-actin-like structures in different tissues (Li et al., 2025). Here we showed that both VLN2
299 and VLN4 proteins had pronounced association with prominent F-actin bundles but less so with
300 fine filaments (Supplemental Figure S2B). Although VLN proteins exhibit common actin-bundling
301 activities in vitro, it will be interesting to determine by live-cell imaging whether these proteins
302 co-localize and if so whether their localization may be augmented by each other *in vivo*. More
303 importantly, we wish to learn how they perform cooperative functions in bundling and/or
304 stabilization of F-actin filaments *in vivo*. Surprisingly, additional mutations in two other *VLN*
305 genes encoding class I and III VLN proteins respectively did not exacerbate the growth
306 phenotypes in the *vln2/3/4* triple mutant (Li et al., 2025), indicating that the three VLN proteins
307 examined in our study play the primary role in F-actin bundling.

308 Previous phenotypic analysis of myosin mutants clearly demonstrated that directional
309 movement of organelles like peroxisomes is dependent on Myosin XI motors (Peremyslov et al.,
310 2010; Perico and Sparkes, 2018). It is intriguing how specific organelles can be actively
311 transported at such a wide range of speeds. We hypothesize that the heterogeneity of
312 peroxisome motility can be brought about by different Myosin XI motors that exhibit different
313 motile activities (Haraguchi et al., 2016). When ectopically expressed in a heterologous system,
314 myosin truncations including the DIL (dilute) domain from at least 7 of the 13 Arabidopsis
315 Myosin XI motors exhibit peroxisome-binding activities (Sattarzadeh et al., 2011). However, it is
316 yet to be determined whether the full-length myosin proteins are associated with the organelle
317 when expressed under their native promoters. It is also possible that multiple motors can bind to
318 the same organelle to increase the movement processivity so that it can be transported for long
319 distance, especially in giant cells of organisms like *Chara corallina* that demonstrate long-
320 distance transport of organelles at great velocities (Shimmen and Yokota, 2004). Varied number
321 of active motors on each peroxisome, which is still hard to quantify *in vivo*, likely contributes to
322 the heterogeneity in transport velocities as well.

323 While Myosin XI motors function as the drive of organelle motility with significant influence on
324 the speed and travel distance, we showed that F-actin organization was critical for the diversity
325 of organelle movement. When VLN-dependent actin bundling is deficient, fewer peroxisomes
326 reached maximum speeds (Figure 3B), and the linearity of peroxisome movement was impaired

327 (Figure 4). Golgi and mitochondria show similar shifts in motility according to the natural
328 variation in F-actin architecture across the root elongation zone (Akkerman et al., 2011). The
329 variation in F-actin networks throughout cell development may support the proper distribution of
330 organelles. For example, longitudinally oriented, prominent F-actin cables are found in plant
331 cells during interphase and are often considered the primary tracks of long-distance transport of
332 organelles for their robust anisotropic expansion (Garcia-González and van Gelderen, 2021).
333 Our analysis of the *vln2/3/4* triple mutant revealed that fine filaments of F-actin are capable of
334 facilitating directional transport of peroxisomes but insufficient to maintain the robust directional
335 movement that takes place on VLN-dependent actin cables. However, the long, stable F-actin
336 bundles exhibit great advantages of promoting rapid, directional movement of the organelles.
337 Compromises of such rapid, directional movement have a profound consequence in cell
338 expansion that presumably is dependent on rapid deployment of organelles across the
339 cytoplasm.

340 In addition to developmentally related roles, both organelle distribution and VLN-dependent
341 actin bundling have been linked to cellular responses to biotic stresses like bacterial infection.
342 For example, inoculation of virulent bacteria induces bundling of F-actin in Arabidopsis leaf cells
343 (Lu et al., 2020; Shimono et al., 2016). It will be very interesting to test whether changes in F-
344 actin organization and/or organelle transport brought about by *vln* mutations influences their
345 susceptibility to pathogenic microbes.

346 We observed highly heterogeneous peroxisome movement, the significance of the which
347 remains unclear. Because peroxisomes often exchange metabolites with other organelles for
348 their function, for example with mitochondria and chloroplasts during photorespiration, it is likely
349 that peroxisome motility is coupled with the position of other organelles to facilitate inter-
350 organelle communication. In fact, chloroplast-mitochondrion-peroxisome interactions increase in
351 response to high light (Jaipargas et al., 2016), which induces higher rates of photorespiration,
352 and mitochondria exhibit different motility patterns before and after being associated with
353 chloroplasts (Oikawa et al., 2021). It would be interesting to determine whether certain
354 movement patterns are unique for peroxisomes physically interacting with other organelles.
355 Additionally, peroxisome velocities may vary across the cytoplasm and are coupled with
356 localized spaces with different physiological conditions. Lastly, various intrinsic and extrinsic
357 factors may cause distinct velocities and directionalities of peroxisomes, which may be enabled
358 by VLN-dependent F-actin bundling for efficient motility and distribution.

359

360 **METHODS AND MATERIALS**

361

362 **Plant genotype and growth**

363

364 *Arabidopsis thaliana* plants were grown in soil in a growth chamber at 21°C with cycles of 16hr
365 light and 8hr dark. *Arabidopsis* seedlings that were used for imaging were sterilized and sowed
366 onto ½ Murashige & Skoog basal media with 0.8% phytagel. Seeds in solid media were cold
367 stratified for 2 days then moved into the growth chamber for 6 days before imaging. All
368 *Arabidopsis thaliana* mutants and WT plants are in the Col-0 genetic background. Floral dipping
369 method was used to deliver transgenes into the plant, following established protocols (Clough
370 and Bent, 1998).

371 Mutants of *VLN4* were isolated from seed stock of SALK_109099C (Arabidopsis Biological
372 Resource Center, Ohio State University), which carried a T-DNA insertion in the 12th intron of the
373 *VLN4* gene, by using the primers 109099RP (5'- CAT TCA AAA ACT CTA TGC TGT TGG-3')
374 and LBb1.3 (5'-GGA TTT TGC CGA TTT CGG AAC CAC-3') to detect the T-DNA insertion and
375 109099LP (5'-TAT ATC TCT GTC ACC TGC CAA AAG-3') and 109099RP to detect the wild-type
376 allele. The *vln2/3* double mutant, generally provided by Prof. Shanjin Huang, was described in
377 an earlier publication (Bao et al., 2012).

378

379 **Plasmid construction**

380

381 To produce an expression vector carrying cassettes for expression of both mScarlet-I-PTS1 and
382 LifeAct-GFP, we first had the codon-optimized mScarlet-I-encoding DNA fragment synthesized
383 commercially (Integrated DNA Technologies, Inc.). The SRL-coding sequence was added to the
384 3' end by PCR using primers 5'- GTA CCG AAT GGT GAG CAA GGG AGA AG-3' and 5'-CGG
385 CGC GCC TTA TAG CCG GCT TTT ATA CAG TTC GTC CAT ACC GCC G-3'. The resulting
386 fragment was inserted into a plasmid containing the promoter sequence of EF1α (AT1G07920).
387 Separately, the LifeAct-coding sequence was synthesized and inserted into pENTR4 (Thermo
388 Fisher), to generate a plasmid expressing LifeAct-GFP under the viral 35S promoter by
389 Gateway LR cloning with the pGWB5 plasmid (Nakagawa et al., 2007). The resulting plasmid

390 was linearized by *Apa*I, after which the DNA fragment for EF1α(p)::mScarlet-I-PTS1 (SRL),
391 amplified by the primers 5'- GCG ACA ATA TGA TCG GGC CTC CGG TGT CAA TCT CAG G-3'
392 and 5'- TGT GGA CGC CGG GCC TTA TAG CCG GCT TTT ATA CAG TTC G-3' from the
393 plasmid described above, was inserted by Gibson reaction to generate the plasmid pLB187
394 used for transformation.

395 Plasmids were transformed into the Agrobacterium strain GV3101, prior to floral dipping in the
396 WT, *vln2/3* and *vln2/3/4* plants.

397

398 **Confocal microscopy**

399

400 After germination and growth in the chambers, Arabidopsis seedlings were mounted in water for
401 imaging. Live-cell imaging was performed on an LSM980 laser scanning confocal microscope
402 with the Airyscan2 function using a 40X water immersion objective and standard excitation and
403 emission settings for EGFP and mCherry by the manufacturer (Carl Zeiss). Single frame images
404 of F-actin were used to measure orientation, coherency, density and skewness. For
405 measurements of F-actin stability, time-lapse images with 5sec/frame were obtained. Similarly,
406 to image peroxisome movement, both markers for F-actin and peroxisomes were
407 simultaneously imaged with a time-lapse of 5sec/frame. At least 3 independent transformant
408 lines were imaged per genotype. In Figure 1A and 3A, time-lapse movies were presented in
409 maximum intensity projection of images collected over time.

410

411 **Quantification of F-actin**

412

413 Images were first rotated such that the direction of hypocotyl growth is along the vertical axis,
414 then thresholded, binarized and skeletonized for F-actin quantification (Higaki, 2017). A region
415 of interest was drawn and selected for quantitative analysis. The ImageJ plugin OrientationJ
416 was used to measure orientation and coherency (Püspöki et al., 2016). Skewness and density
417 were measured using the LPX plugin package (Higaki et al., 2010; Schneider et al., 2012).

418 In measuring the percentage of stable F-actin, F-actin was imaged for 10 sec at 5 sec/frame,
419 after which the first (time zero) and the last (10 sec) frames were merged. Under the reasoning

420 that stable F-actin filaments should still be present or unchanged in position after 10 sec, a
421 stable filament from the last frame should colocalize with itself from the first frame. The merged
422 image was thresholded for colocalized filaments. The percentage of stable F-actin was
423 calculated using the ratio of colocalized F-actin signal to the total F-actin signal.

424

425 **Quantification of peroxisome motility and distribution**

426

427 Quantitative measurement of F-actin-dependent peroxisome motility was carried out by imaging
428 F-actin and peroxisomes simultaneously with 5-sec intervals. Peroxisomes not associated with
429 F-actin were not measured. Peroxisomes were tracked using the ImageJ plugin, TrackMate
430 (Ershov et al., 2022). Given that the speed of slow moving peroxisomes is usually ≥0.2 μm/sec
431 (Mathur et al., 2002), we excluded peroxisomes moving at velocities below 0.1 μm/sec as those
432 appear to be more likely due to Brownian movements. We also manually reevaluated the tracks
433 with velocities <0.1 μm/sec to confirm that these movements appeared oscillatory. The output
434 track data summarized the overall movement of individual peroxisomes during the imaging
435 duration, and provided the following track features: (1) mean speed for the average speed
436 values during every 5-sec intervals along a track; (2) maximum speed for the highest
437 instantaneous speed between two consecutive timepoints along a track; (3) straight-line speed,
438 calculated as track displacement divided by track duration; (4) total distance traveled; (5) track
439 displacement; (6) linearity of forward progression for the ratio between straight-line speed and
440 track mean speed, where completely linear tracks would have a value of 1; and (7) directional
441 change rate calculated as the average angle between consecutive timepoints along a track
442 divided by the track duration.

443 To quantify peroxisome distribution, a dispersion ratio was calculated by having the track
444 displacement (μm) divided by the directional change rate (rad/s). A higher ratio represents
445 peroxisomes that travel long distances with few turns, which would result in peroxisome
446 dispersion across the cell. A lower ratio represents a peroxisome that turns frequently and
447 moves within a small region.

448

449 **Acknowledgements**

We thank Dr. Shanjin Huang for providing the *vln2/3* mutant seeds and Dr. Tsuyoshi Nakagawa for sharing the pGWB plasmids, Dr. Felicia L. Peng and Dr. Chenxin Li for their advice and comments on this work. This study was made possible in part through access to the MCB Light Microscopy Core Facility with training and support by Dr. Thomas Wilkop.

Competing interests

The authors declare no other competing or financial interests.

Author contributions

Conceptualization: C.H.H., Y.-R.J.L., J.H., B.L.; Methodology: C.H.H., A.M.K., Y.-R.J.L., J.H., B.L.; Investigation: C.H.H., Y.-R.J.L.; Formal analysis: C.H.H., A.M.K., Y.-R.J.L.; Visualization: C.H.H., Y.-R.J.L.; Data curation: C.H.H.; Supervision: B.L., J.H.; Project administration: B.L.; Funding acquisition: J.H., B.L.; Writing (original draft): C.H.H., A.M.K.; Writing (review and editing): C.H.H., A.M.K., Y.-R.J.L., J.H., B.L.

Funding

This work was supported by grants from the U.S. National Science Foundation (2148207 to B.L & 2148206 to J.H). B.L. was also sponsored by the U.S. Department of Agriculture (USDA)-the National Institute of Food and Agriculture (NIFA) under an Agricultural Experiment Station (AES) hatch project (CA-D-PLB-2536-H). A.M.K was partially funded by a grant from the Chemical Sciences, Geoscience and Biosciences Division, Office of Basic Energy Sciences, Office of Science, U.S. Department of Energy (DE-FG02-91ER20021) to J.H. The Zeiss LSM 980 microscope used in this study was purchased with a grant (S10OD026702) from the U.S. National Institutes of Health.

Data and resource availability

All data acquired from this study are included within the main text and Supplementary information.

FIGURE LEGENDS

Figure 1. F-actin organization in the Arabidopsis *vln* mutants. (A) LifeAct-GFP-labeled F-actin imaged at the cell cortex of hypocotyl epidermal cells in transgenic wild-type (WT), *vln2/3*, and *vln2/3/4* plants. The WT cell has cortical F-actin in two populations: long, thick bundles and finer filaments in mesh network. The prominent bundles are reduced in *vln2/3* and almost completely lost in *vln2/3/4*. Maximum projections of the LifeAct-GFP images taken over time are shown for all genotypes. (B) The skewness of the F-actin as a measurement of how well the filaments are bundled. Values were obtained from n>35 cells of each genotype. (C) Quantitative assessment of F-actin orientation, determined as the angle relative to the reference axis, where 90° angle is parallel to the direction of growth indicated by double arrows in (A). The mean values are indicated by thick dotted lines. Significance is determined by a two-tailed t-test with $p < 0.01$ (****). Scale bar: 5 μm.

Figure 2. Effects of *vln* mutations on the dynamics of F-actin in Arabidopsis. (A) Three time-lapse images of F-actin taken at 5-sec intervals in the WT, *vln2/3*, and *vln2/3/4* cells. In the merged images, each frame is pseudo-colored (red at 0 sec, green at 5 sec, and blue at 10 sec) to reflect the changes of F-actin filaments where stable filaments with no changes after 10 sec appear in white. WT cells have more stable filaments, whereas the double mutant *vln2/3* has fewer stable filaments and the triple mutant *vln2/3/4* mostly has rapidly remodeling of F-actin filaments. (B) Quantification of the amount of stable F-actin. WT has the highest amount while the *vln2/3* and *vln2/3/4* mutants progressively have less. Values are measured from n>35 cells of each genotype. (C) Coherency of F-actin filaments as a measurement of how F-actin filaments are aligned. Higher coherency values represent more ordered filaments in a preferred direction. (D) Comparison of F-actin density in WT, *vln2/3*, and *vln2/3/4* cells. Density value is determined by the proportion (%) of the cell cortex occupied by F-actin. Significance is determined by a two-tailed t-test with $p < 0.01$ (****). Scale bar: 5 μm.

Figure 3. Peroxisome motility is affected in the *vln2/3/4* mutant lacking F-actin bundling. (A) Maximum projections over time of peroxisome and F-actin simultaneously imaged at 5-sec intervals. In the *vln2/3* and *vln2/3/4* mutant cells that have reduced long F-actin bundles, peroxisomes show aggregation, impaired distribution, and reduced linear movement. (B-C) Quantitative assessments of average peroxisome speed and maximum speed in WT and *vln* mutants. Values are measured from n>300 peroxisome tracks from each genotype and plotted along a raincloud plot with a histogram on top and a boxplot below. Yellow diamonds represent the mean position. Statistical significance is determined by a Wilcoxon rank sum test with p-values shown in the figures.

516 **Figure 4**. Quantitative comparison of peroxisome tracks in the WT, *vln2/3* and *vln2/3/4* mutant
517 cells. Parameters include total distance (A), track displacement (B), average straight-line speed
518 (C), linearity as a ratio of straight-line speed to track mean speed (D), and directional change
519 rate in radians (rad)/s (E). Values are obtained from n>300 peroxisome tracks from each
520 genotype and plotted in a raincloud plot with a histogram on top and a boxplot below. Yellow
521 diamonds represent the mean values. Significance is determined by a Wilcoxon rank sum test
522 with p-values shown in the figures.

523

524 **Figure 5.** Multivariate clustering and dispersion analysis distinguish peroxisome movement
525 behaviors in WT and *vln* mutants. (A) Pairwise correlation analysis of peroxisome movement in
526 directional change rate, average straightforward speed, and linearity. Formation of three clusters
527 resulted from the pairwise correlation analysis. Proportion of peroxisome movement patterns is
528 represented by the three clusters in WT, *vln2/3*, and *vln2/3/4* cells. (B) Peroxisome dispersion
529 ratios used to quantify peroxisome distribution, as reflected by the rate of track displacement
530 and directional change [μm/(rad/sec)]. Peroxisomes in WT and *vln2/3* are able to travel long
531 distances before changing directions, shown by higher ratio values. Conversely, peroxisomes in
532 *vln2/3/4* show more confined movements within a localized region, evidenced by lower ratio
533 values when compared to WT and *vln2/3*. Significance is determined by a two-tailed t-test with
534 p-values shown in the figures. Values are measured from n>300 peroxisomes for each
535 genotype.

REFERENCES

Akkerman, M., Overdijk, E. J. R., Schel, J. H. N., Emons, A. M. C. and Ketelaar, T. (2011). Golgi Body Motility in the Plant Cell Cortex Correlates with Actin Cytoskeleton Organization. *Plant and Cell Physiology* **52**, 1844-1855.

Avisar, D., Prokhnevsky, A. I., Makarova, K. S., Koonin, E. V. and Dolja, V. V. (2008). Myosin XI-K Is required for rapid trafficking of Golgi stacks, peroxisomes, and mitochondria in leaf cells of Nicotiana benthamiana. *Plant Physiol* **146**, 1098-108.

Bao, C. C., Wang, J., Zhang, R. H., Zhang, B. C., Zhang, H., Zhou, Y. H. and Huang, S. J. (2012). Arabidopsis VILLIN2 and VILLIN3 act redundantly in sclerenchyma development via bundling of actin filaments. *Plant Journal* **71**, 962-975.

Clough, S. J. and Bent, A. F. (1998). Floral dip: a simplified method for Agrobacterium-mediated transformation of *Arabidopsis thaliana*. *Plant J* **16**, 735-743.

Covill-Cooke, C., Toncheva, V. S. and Kittler, J. T. (2021). Regulation of peroxisomal trafficking and distribution. *Cellular And Molecular Life Sciences* **78**, 1929-1941.

Ershov, D., Phan, M.-S., Pylvänäinen, J. W., Rigaud, S. U., Le Blanc, L., Charles-Orszag, A., Conway, J. R. W., Laine, R. F., Roy, N. H., Bonazzi, D. et al. (2022). TrackMate 7: integrating state-of-the-art segmentation algorithms into tracking pipelines. *Nature Methods* **19**, 829-832.

Garcia-González, J. and van Gelderen, K. (2021). Bundling up the Role of the Actin Cytoskeleton in Primary Root Growth. *Front Plant Sci* **12**.

Haraguchi, T., Tominaga, M., Nakano, A., Yamamoto, K. and Ito, K. (2016). Myosin XI-I is Mechanically and Enzymatically Unique Among Class-XI Myosins in Arabidopsis. *Plant Cell Physiol* **57**, 1732-43.

He, A. Y., Dean, J. M. and Lodhi, I. J. (2021). Peroxisomes as cellular adaptors to metabolic and environmental stress. *Trends in Cell Biology* **31**, 656-670.

Henty-Ridilla, J. L., Li, J. J., Blanchoin, L. and Staiger, C. J. (2013). Actin dynamics in the cortical array of plant cells. *Current Opinion in Plant Biology* **16**, 678-687.

Higaki, T. (2017). Quantitative evaluation of cytoskeletal organizations by microscopic image analysis. *PLANT MORPHOLOGY* **29**, 15-21.

Higaki, T., Kutsuna, N., Sano, T., Kondo, N. and Hasezawa, S. (2010). Quantification and cluster analysis of actin cytoskeletal structures in plant cells: role of actin bundling in stomatal movement during diurnal cycles in Arabidopsis guard cells. *Plant Journal* **61**, 156-165.

Huang, S., Qu, X. and Zhang, R. (2015). Plant villins: versatile actin regulatory proteins. *J Integr Plant Biol* **57**, 40-9.

Jaipargas, E. A., Mathur, N., Daher, F. B., Wasteneys, G. O. and Mathur, J. (2016). High light intensity leads to increased peroxule-mitochondria interactions in plants. *Front Cell Dev Biol* **4**.

Khurana, P., Henty, J. L., Huang, S. J., Staiger, A. M., Blanchoin, L. and Staiger, C. J. (2010). VILLIN1 and VILLIN3 Have Overlapping and Distinct Activities in Actin Bundle Formation and Turnover. *Plant Cell* **22**, 2727-2748.

579 **Koenig, A. M., Liu, B. and Hu, J. P.** (2023). Visualizing the dynamics of plant energy
580 organelles. *Biochemical Society Transactions* **51**, 2029-2040.
581 **Li, X., Zhuang, Y. H., Zhao, W. Y., Qu, X. L., Wang, J., Chang, M., Shen, J. F., Chen,**
582 **N. Z. and Huang, S. J.** (2025). Molecular and functional adaption of Arabidopsis villins.
583 *New Phytologist* **245**, 1158-1179.
584 **Lu, Y. J., Li, P., Shimono, M., Corrion, A., Higaki, T., He, S. Y. and Day, B.** (2020).
585 Arabidopsis calcium-dependent protein kinase 3 regulates actin cytoskeleton organization
586 and immunity. *Nature Communications* **11**.
587 **Mathur, J., Mathur, N. and Hulskamp, M.** (2002). Simultaneous visualization of
588 peroxisomes and cytoskeletal elements reveals actin and not microtubule-based
589 peroxisome motility in plants. *Plant Physiol* **128**, 1031-45.
590 **Nakagawa, T., Kurose, T., Hino, T., Tanaka, K., Kawamukai, M., Niwa, Y., Toyooka,**
591 **K., Matsuoka, K., Jinbo, T. and Kimura, T.** (2007). Development of series of gateway binary
592 vectors, pGWBs, for realizing efficient construction of fusion genes for plant
593 transformation. *J Biosci Bioeng* **104**, 34-41.
594 **Neuhaus, A., Eggeling, C., Erdmann, R. and Schliebs, W.** (2016). Why do
595 peroxisomes associate with the cytoskeleton? *Biochimica Et Biophysica Acta-Molecular*
596 *Cell Research* **1863**, 1019-1026.
597 **Oikawa, K., Imai, T., Thagun, C., Toyooka, K., Yoshizumi, T., Ishikawa, K.,**
598 **Kodama, Y. and Numata, K.** (2021). Mitochondrial movement during its association with
599 chloroplasts in. *Communications Biology* **4**.
600 **Pan, R. H., Liu, J., Wang, S. S. and Hu, J. P.** (2020). Peroxisomes: versatile
601 organelles with diverse roles in plants. *New Phytologist* **225**, 1410-1427.
602 **Peremyslov, V. V., Prokhnevsky, A. I. and Dolja, V. V.** (2010). Class XI myosins are
603 required for development, cell expansion, and F-Actin organization in Arabidopsis. *Plant*
604 *Cell* **22**, 1883-97.
605 **Perico, C. and Sparkes, I.** (2018). Plant organelle dynamics: cytoskeletal control
606 and membrane contact sites. *New Phytologist* **220**, 381-394.
607 **Püspöki, Z., Storath, M., Sage, D. and Unser, M.** (2016). Transforms and Operators
608 for Directional Bioimage Analysis: A Survey. *Focus on Bio-Image Informatics* **219**, 69-93.
609 **Salogiannis, J. and Reck-Peterson, S. L.** (2017). Hitchhiking: A Non-Canonical
610 Mode of Microtubule-Based Transport. *Trends in Cell Biology* **27**, 141-150.
611 **Sandalio, L. M., Peláez-Vico, M. A., Molina-Moya, E. and Romero-Puertas, M. C.**
612 (2021). Peroxisomes as redox-signaling nodes in intracellular communication and stress
613 responses. *Plant Physiology* **186**, 22-35.
614 **Sattarzadeh, A., Schmelzer, E. and Hanson, M. R.** (2011). Analysis of Organelle
615 Targeting by DIL Domains of the Arabidopsis Myosin XI Family. *Front Plant Sci* **2**, 72.
616 **Schneider, C. A., Rasband, W. S. and Eliceiri, K. W.** (2012). NIH Image to ImageJ:
617 25 years of image analysis. *Nat Methods* **9**, 671-675.
618 **Shimmen, T. and Yokota, E.** (2004). Cytoplasmic streaming in plants. *Curr Opin*
619 *Cell Biol*. **16**, 68-72.
620 **Shimono, M., Lu, Y. J., Porter, K., Kvitko, B. H., Henty-Ridilla, J., Creason, A., He,**
621 **S. Y., Chang, J. H., Staiger, C. J. and Day, B.** (2016). The type III effector HopG1 induces

622 actin remodeling to promote symptom development and susceptibility during infection.
623 *Plant Physiology* **171**, 2239-2255.
624 **van der Honing, H. S., Kieft, H., Emons, A. M. C. and Ketelaar, T.** (2012).
625 Arabidopsis VILLIN2 and VILLIN3 Are Required for the Generation of Thick Actin Filament
626 Bundles and for Directional Organ Growth. *Plant Physiology* **158**, 1426-1438.
627 **Wanders, R. J. A., Baes, M., Ribeiro, D., Ferdinandusse, S. and Waterham, H. R.**
628 (2023). The physiological functions of human peroxisomes. *Physiol Rev* **103**, 957-1024.
629 **Yokota, E., Vidali, L., Tominaga, M., Tahara, H., Orii, H., Morizane, Y., Hepler, P. K.**
630 **and Shimmen, T.** (2003). Plant 115-kDa actin-filament bundling protein, P-115-ABP, is a
631 homologue of plant villin and is widely distributed in cells. *Plant and Cell Physiology* **44**,
632 1088-1099.

633

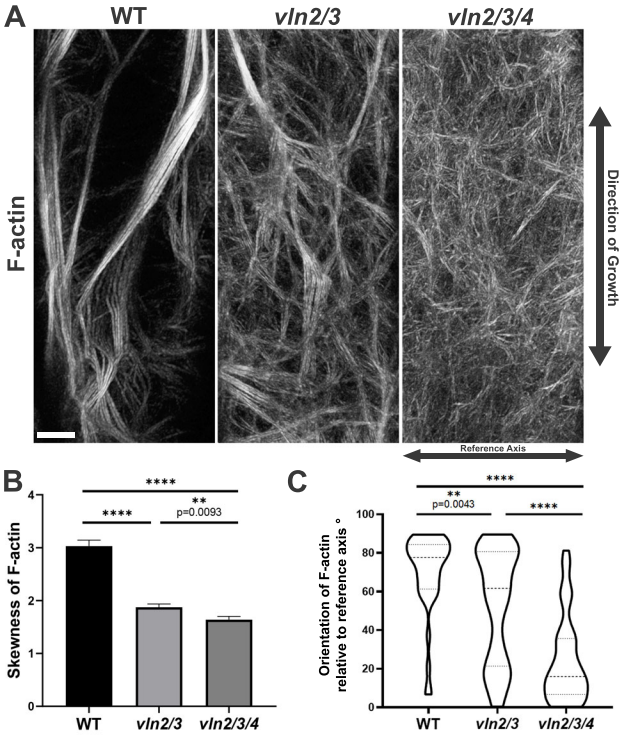
A
WT
vln2/3
vln2/3/4
F-actin
Direction of Growth
Reference Axis
B
Skewness of F-actin
****
****
**
p=0.0093
WT
vln2/3
vln2/3/4
C
Orientation of F-actin relative to reference axis °
****
**
p=0.0043
****
WT
vln2/3
vln2/3/4

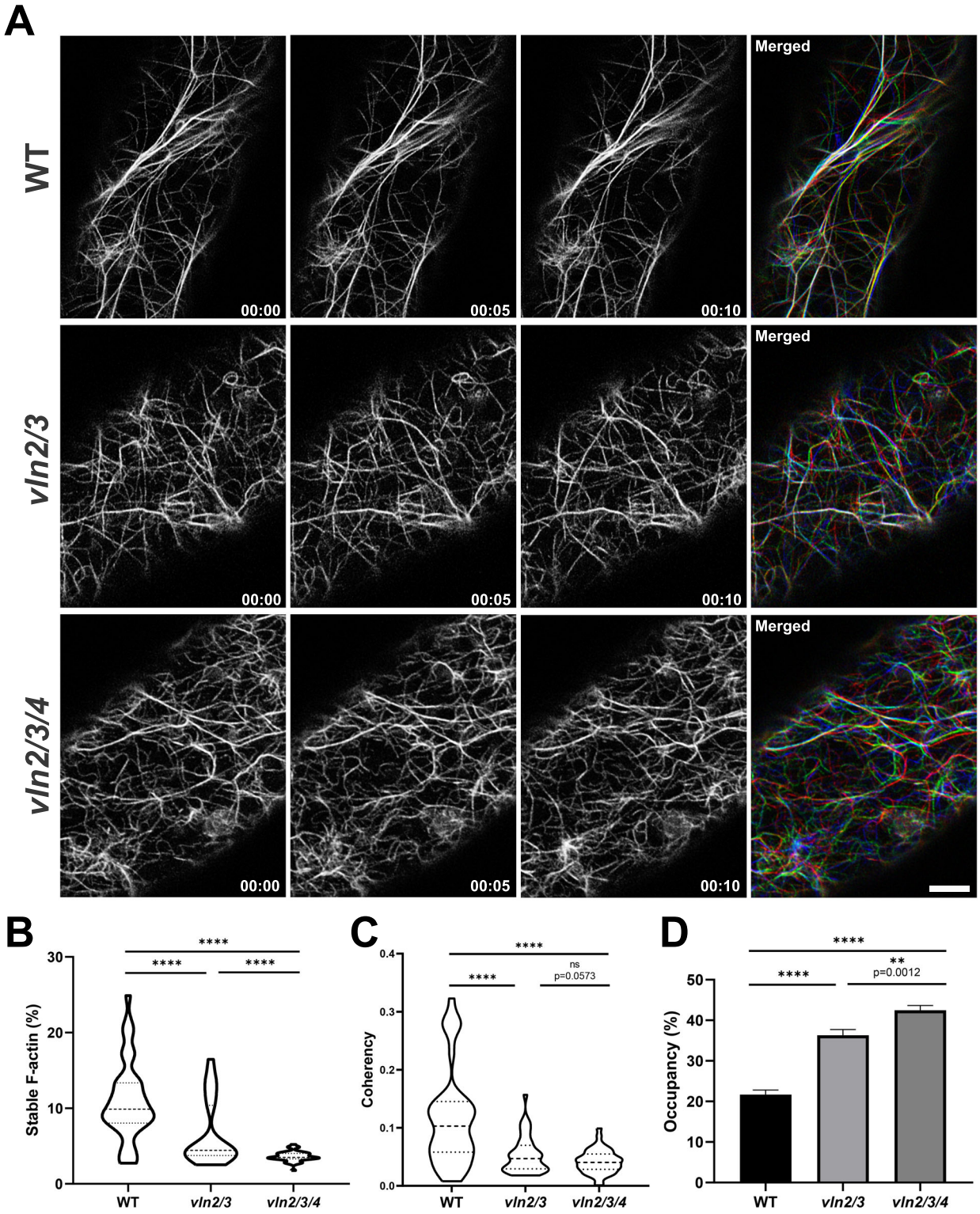
A
WT
vln2/3
vln2/3/4
Merged
00:00
00:05
00:10
B
Stable F-actin (%)
****
****
****
WT
vln2/3
vln2/3/4
C
Coherency
****
****
ns
p=0.0573
D
Occupancy (%)
****
**
p=0.0012

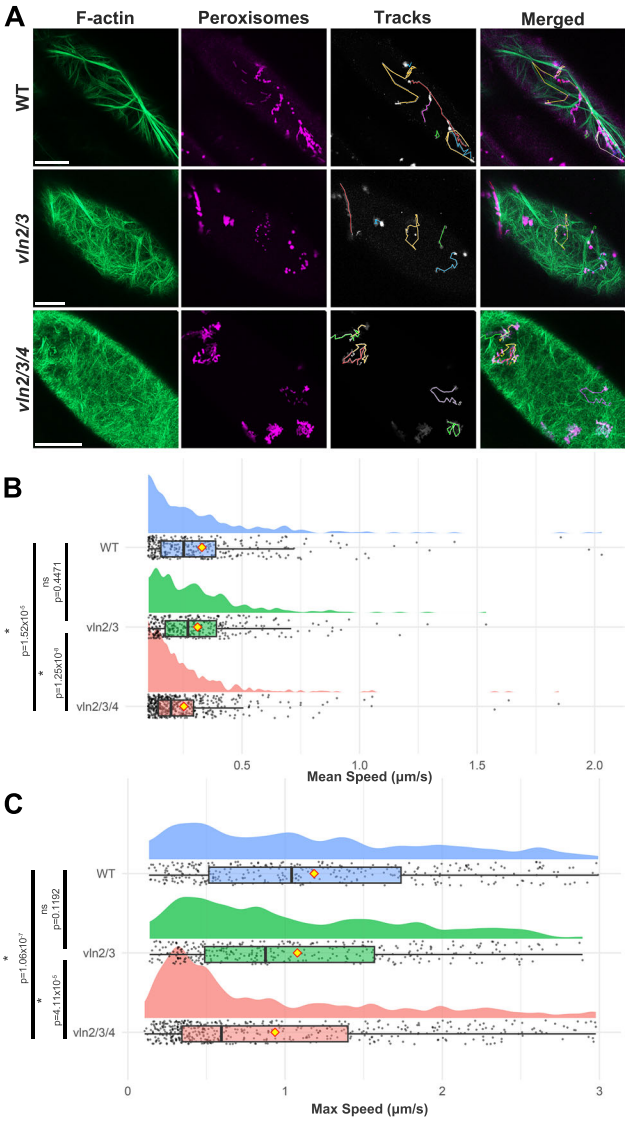
A
F-actin
Peroxisomes
Tracks
Merged
WT
vIn2/3
vIn2/3/4
B
WT
vIn2/3
vIn2/3/4
*
p=1.52x10^-5
ns
p=0.4471
*
p=1.25x10^-8
0.5
1.0
1.5
2.0
Mean Speed (µm/s)
C
WT
vIn2/3
vIn2/3/4
*
p=1.06x10^-7
ns
p=0.1192
*
p=4.11x10^-5
0
1
2
3
Max Speed (µm/s)

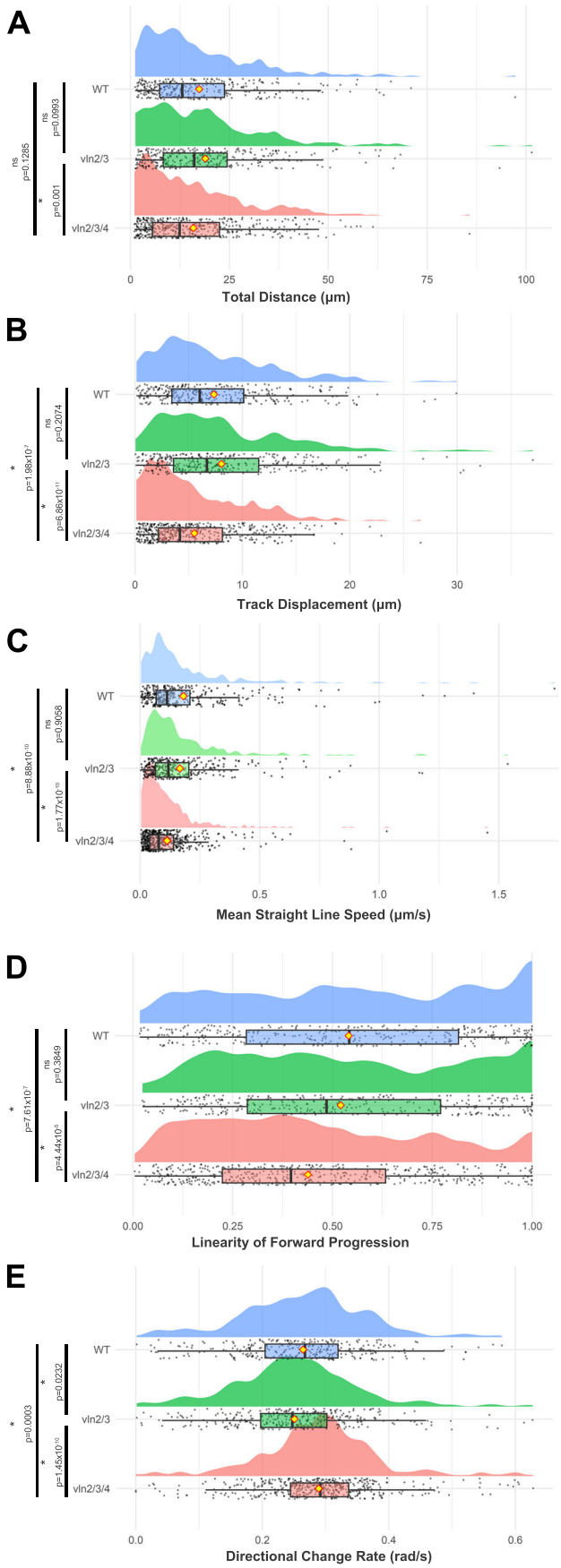
A
WT
vIn2/3
vIn2/3/4
ns
p=0.1295
ns
p=0.0993
*
p=0.001
0
25
50
75
100
Total Distance (µm)
B
WT
vIn2/3
vIn2/3/4
*
p=1.98x10⁻⁷
ns
p=0.2074
*
p=6.86x10⁻¹¹
0
10
20
30
Track Displacement (µm)
C
WT
vIn2/3
vIn2/3/4
*
p=8.88x10⁻¹⁰
ns
p=0.9058
*
p=1.77x10⁻¹⁰
0.0
0.5
1.0
1.5
Mean Straight Line Speed (µm/s)
D
WT
vIn2/3
vIn2/3/4
*
p=7.61x10⁻⁷
ns
p=0.3849
*
p=4.44x10⁻⁵
0.00
0.25
0.50
0.75
1.00
Linearity of Forward Progression
E
WT
vIn2/3
vIn2/3/4
*
p=0.0003
*
p=0.0232
*
p=1.45x10⁻¹⁰
0.0
0.2
0.4
0.6
Directional Change Rate (rad/s)

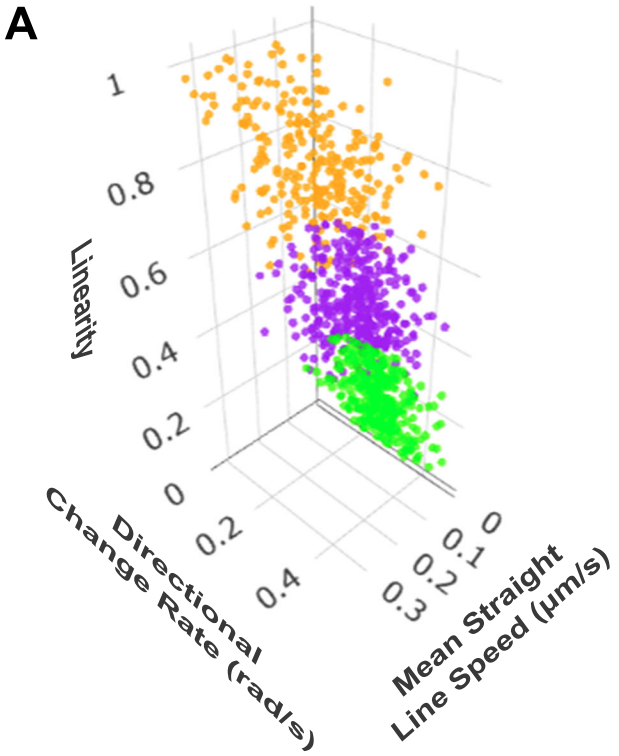
A
Linearity
1
0.8
0.6
0.4
0.2
0
Directional Change Rate (rad/s)
0.2
0.4
Mean Straight Line Speed (µm/s)
0
0.1
0.2
0.3

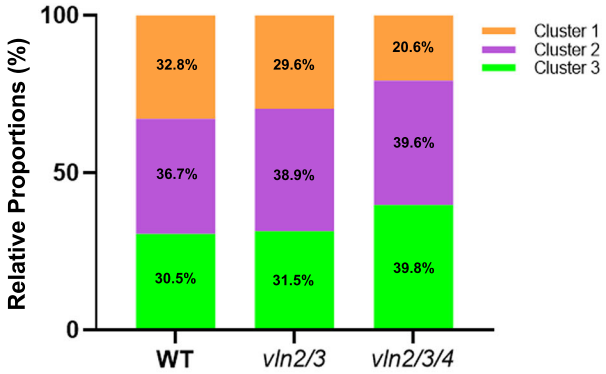
Relative Proportions (%)
100
50
0
32.8%
36.7%
30.5%
29.6%
38.9%
31.5%
20.6%
39.6%
39.8%
WT
vln2/3
vln2/3/4
Cluster 1
Cluster 2
Cluster 3

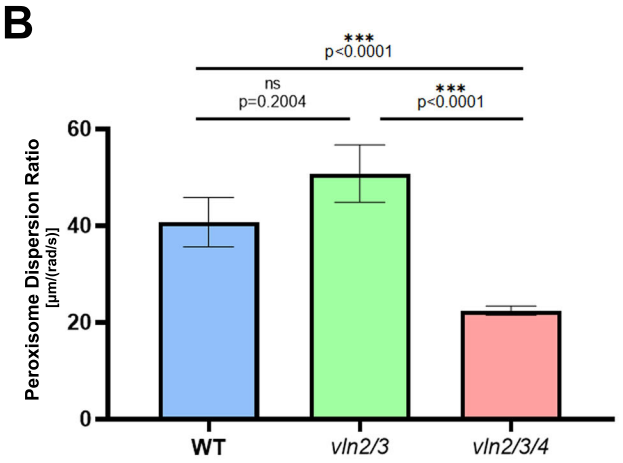
B
***
p<0.0001
ns
p=0.2004
***
p<0.0001
Peroxisome Dispersion Ratio
[µm/(rad/s)]
60
40
20
0
WT
vln2/3
vln2/3/4